IEEE Access
Multidisciplinary | Rapid Review | Open Access Journal

Received April 27, 2020, accepted May 6, 2020, date of publication May 12, 2020, date of current version May 22, 2020.

Digital Object Identifier 10.1109/ACCESS.2020.2994083

On the Performance of GFDM Assisted NOMA Schemes

XIAOTONG ZHANG, ZHENDUO WANG, (Member, IEEE), XIAOYAN NING, AND HONG XIE
College of Information and Communication Engineering, Harbin Engineering University, Harbin 150001, China

Corresponding author: Zhenduo Wang (zhenduowang@hrbeu.edu.cn)

This work was supported in part by the Fundamental Research Funds for the Central Universities under Grant 3072020CFJ0802.

ABSTRACT From the points of spectral efficiency, low latency and massive connectivity, novel modulation and multiple access schemes have been proposed in fifth generation (5G) wireless networks. However, the combinations of multiplexing and multiple access techniques have not been widely investigated in most literatures. Therefore, we joint generalized frequency division multiplexing (GFDM) waveforms and power-domain non-orthogonal multiple access (NOMA) systems together in order to further extend the framework of multi-carrier NOMA, and also achieve performance evaluations for NOMA networks with one base station and two users. Basically, theoretical BER expressions of downlink and uplink GFDM assisted NOMA schemes are mathematically derived and then verified by simulation results. In addition, combined performance advantages, including higher achievable sum rate, lower peak-to-average power ratio (PAPR) and out of band power (OOBP) radiation, can be obtained in GFDM assisted NOMA networks.

INDEX TERMS 5G, generalized frequency division multiplexing (GFDM), non-orthogonal multiple access (NOMA), multi-carrier NOMA, theoretical BER.

I. INTRODUCTION

Non-orthogonal multiple access (NOMA) has become an indispensable technology for fifth-generation (5G) wireless cellular networks with massive connectivity and high throughput [1]–[4], especially for machine-type communications (MTC) applications in [5]. Existing NOMA schemes could be achieved in power-domain, code-domain or multiple domains multiplexing. In addition, superposition coding (SC) is employed in power-domain NOMA (PD-NOMA) to transmit multiple users' information within one time-frequency resource block. The multiuser in downlink is distinguished through allocating different power, and successive interference cancellation (SIC) is utilized at the receiver to successively decode data of different users. In NOMA networks, on one hand, sum rate is a key indicator to evaluate performances. On the other hand, it is also essential to theoretically study BER performances. For instance, theoretical BER expressions of downlink and uplink NOMA systems are investigated in [6]–[9] and [9]–[11], respectively.

The SC in power-domain is usually applied to a single resource block, i.e. single carrier NOMA. Furthermore, the principle of multi-carrier NOMA is introduced in [12]–[15], which combines orthogonal frequency division multiplexing (OFDM) with NOMA. It is worth noting that high peak-to-average power ratio (PAPR) and out of band power (OOBP) radiation are main drawbacks of OFDM based systems. In order to overcome shortcomings of OFDM systems, novel waveforms [16]–[18], such as filter bank-based multi-carrier (FBMC), generalized frequency division multiplexing (GFDM), universal filtered multi-carrier (UFMC) and filtered OFDM systems, have been proposed to achieve lower OOBP, higher spectral efficiency and stronger flexibility. As a result, several literatures focus on combinations of novel multiple access and multiplexing technologies, such as SCMA with GFDM in [19], PDMA with FBMC in [20], and NOMA with UFMC in [21] to achieve combined performance advantages. However, comprehensive performance evaluations of GFDM assisted PD-NOMA schemes have not been widely investigated in previous literatures, especially for theoretical BER analysis of uplink and downlink networks.

In this paper, therefore, we joint GFDM waveforms with NOMA schemes to extend the framework of multi-carrier NOMA networks. Primarily, theoretical BER expressions of two users are derived for downlink and uplink GFDM assisted NOMA schemes. Furthermore, achievable sum rate, PAPR and OOBP performances are also evaluated to illustrate combined performance advantages of united systems.

The associate editor coordinating the review of this manuscript and approving it for publication was Di Zhang.

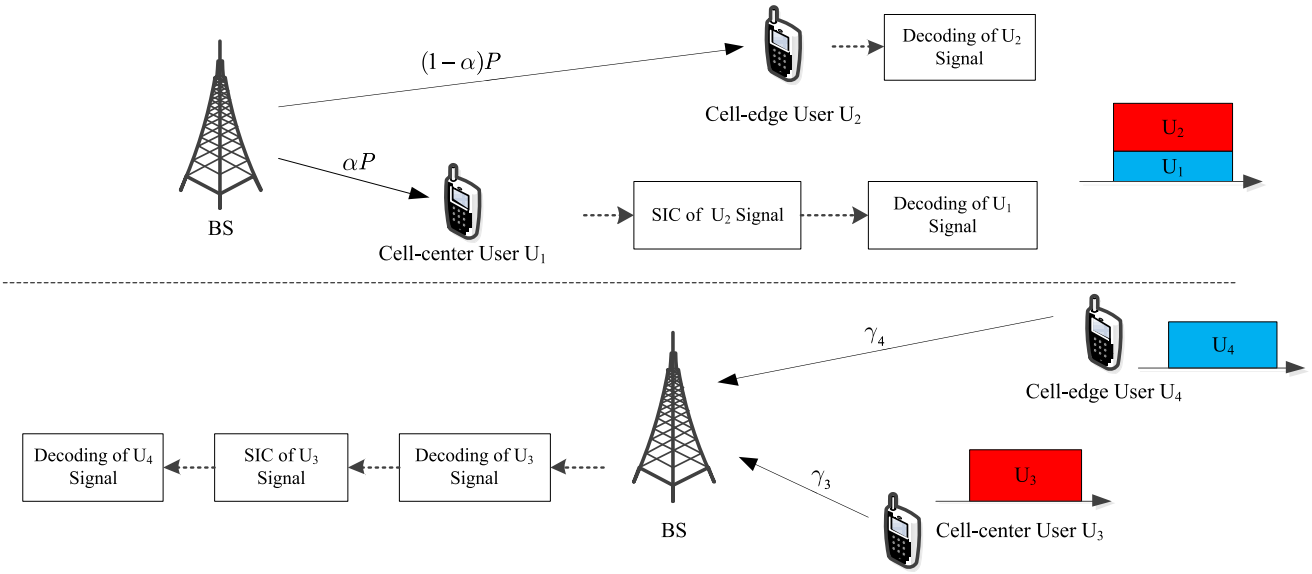

FIGURE 1. Framework of downlink and uplink NOMA networks.

II. BASIC CONCEPTS

A. A TYPICAL DOWNLINK NOMA SCHEME

As shown in Fig.1, a downlink NOMA scenario with one base station (BS) and two users is considered, where U_1 and U_2 are cell-center user and cell-edge user, i.e. near user and far user, respectively. At the BS, SC is implemented to transmit information within one time-frequency resource block with different power, and transmitted data is expressed as

$$s=\sqrt{P_1}\cdot s_1+\sqrt{P_2}\cdot s_2=\sqrt{\alpha P}\cdot s_1+\sqrt{(1-\alpha)P}\cdot s_2, \quad (1)$$

where the total power P is assumed to be unit energy for the convenience of analysis. The power allocation factor (PAF) is α with $P_1 = \alpha P$ and $P_2 = (1-\alpha)P$. s_1 and s_2 denote transmitted signals from BS to U_1 and U_2, respectively. The received signal at U_θ is

$$r_\theta = h_\theta \cdot s + v_\theta, \quad \theta = 1, 2, \quad (2)$$

where h_θ and v_θ are channel responses with $|h_1|^2 > |h_2|^2$ and AWGN with variance σ_v^2. It means that the near user has stronger channel conditions than far user. Thereby, lower transmit power is always allocated to the stronger user, and more power is given to the weaker user.

At the user side, the signal of U_2, as a result of greater share of transmit power, is firstly decoded by considering the signal of U_1 as interference. After that, the information of U_1 can be decoded by performing SIC to remove U_2 from the received signal, expressed as

$$r_1=\sqrt{P_1}\cdot h_1\cdot s_1+\sqrt{P_2}\cdot h_1\cdot s_2-\sqrt{P_2}\cdot h_1\cdot \bar{s}_2+v_1, \quad (3)$$

where $\bar{s}_2$ denotes demodulated signal of U_2 and we assume complete channel state information (CSI) is available.

As given in [4], the achievable data rate of U_2 is

$$R_{NOMA,U_2} = \log_2\left(1+\frac{P_2|h_2|^2}{P_1|h_2|^2+\sigma_v^2}\right). \quad (4)$$

Considering the case of perfect SIC, the achievable data rate for U_1 is

$$R_{NOMA,U_1} = \log_2\left(1+\frac{P_1|h_1|^2}{\sigma_v^2}\right). \quad (5)$$

Therefore, the achievable sum rate of NOMA networks with two users could be calculated as

$$\begin{aligned} R_{NOMA,sum} &= R_{NOMA,U_1} + R_{NOMA,U_2} \\ &= \log_2\left(1+\frac{P_1|h_1|^2}{\sigma_v^2}\right) \\ &\quad + \log_2\left(1+\frac{P_2|h_2|^2}{P_1|h_2|^2+\sigma_v^2}\right). \end{aligned} \quad (6)$$

B. A TYPICAL UPLINK NOMA SCHEME

Similar as downlink NOMA networks, we also consider one BS and two users in an uplink NOMA scenario in Fig.1, where U_3 and U_4 are cell-center user and cell-edge user, respectively. The received signal at the BS is expressed as

$$r_{UL} = h_3\cdot s_3 + h_4\cdot s_4 + v, \quad (7)$$

where h_3 and h_4 denote channel responses between BS and users. The transmitted power of near user U_3 and far user U_4 is P_3 and P_4, respectively. At the BS, the SIC is still employed to decode received data of U_3 and U_4. As a result of less path loss, it is usually assumed that $P_3|h_3|^2 > P_4|h_4|^2$, which is different from the downlink demodulation process. Therefore, the near user is firstly decoded and then far user is successively decoded after removing interference of U_3. According to SIC strategy, the information of U_4 can be decoded as

$$r_4 = h_3\cdot s_3 - h_3\cdot \bar{s}_3 + h_4\cdot s_4 + v, \quad (8)$$

where $\bar{s}_3$ is the decoded signal of U_3. Therefore, there is a couple of differences between downlink and uplink NOMA networks, especially for the decoding order of users.

C. GFDM SYSTEMS

As shown in [22], in GFDM systems with total $N = MK$ transmitted data, there are K subcarriers with M subsymbols on each subcarrier shaped by filter $g_{k,m}(n)$, which is expressed as

$$g_{k,m}[n] = g[(n - mK) \text{mod} N] \cdot \exp\left[-j2\pi \frac{k}{K} n\right], \quad (9)$$

where k and m denote kth subcarrier and mth subsymbol. Each pulse shape filter $g_{k,m}[n]$ with sampling index n is a time and frequency shifted version of prototype raised $g[n]$, and thus transmitted data is calculated as

$$x[n] = \sum_{k=0}^{K-1} \sum_{m=0}^{M-1} d_{k,m} g_{k,m}[n]. \quad (10)$$

The matrix form of modulation process in (10) can be expressed as $\mathbf{x} = \mathbf{A} \cdot \mathbf{d}$, where modulation matrix $\mathbf{A}$ is denoted as $\mathbf{A} = (\mathbf{g}_{0,0} \cdots \mathbf{g}_{K-1,0} \mathbf{g}_{0,1} \cdots \mathbf{g}_{K-1,M-1})$, and columns of $\mathbf{A}$ are given by $\mathbf{g}_{k,m} = (g_{k,m}[n])^T$.

Considering demodulator $\mathbf{B}$ at the receiver, analytical BER expressions of GFDM systems are derived by calculating the noise enhancement factor (NEF) at the receiver, which leads to deteriorated BER performances in comparison with OFDM systems. The received signal after fading channels is

$$\mathbf{y}_{GFDM} = \mathbf{B} \cdot \mathbf{\Lambda}^{-1} \cdot (\mathbf{\Lambda} \cdot \mathbf{A} \cdot \mathbf{d} + \mathbf{v}) = \mathbf{d} + \mathbf{B} \cdot \mathbf{\Lambda}^{-1} \cdot \mathbf{v}, \quad (11)$$

where the frequency domain response of fading channels is represented as $\mathbf{\Lambda} = \text{diag}([\lambda_0, \lambda_1, \ldots, \lambda_{N-1}]^T)$. The zero forcing (ZF) receiver $\mathbf{B} = \mathbf{A}^{-1}$ could be obtained in [23] through utilizing dual Gabor window. In order to count equivalent noise at the receiver, the NEF is calculated as

$$\xi_F = \frac{1}{N} \sum_{k=0}^{N-1} \sum_{i=0}^{N-1} |\mathbf{B} \cdot \mathbf{\Lambda}^{-1}|_{k,i}^2 = \frac{1}{N} \sum_{k=0}^{N-1} \sum_{i=0}^{N-1} \frac{|\mathbf{B}|_{k,i}^2}{|\lambda_i|^2}, \quad (12)$$

and thus the enhanced noise is given as $\sigma_{GFDM,v}^2 = \xi_F \cdot \sigma_v^2$. For AWGN channels, there is

$$\xi_{AWGN} = \frac{1}{N} \sum_{k=0}^{N-1} \sum_{i=0}^{N-1} |\mathbf{B}|_{k,i}^2 \doteq \xi. \quad (13)$$

According to calculated NEF in (12), analytical BER expression with ZF receiver is derived as

$$\mathcal{P}_{b,GFDM} = Q\left(\sqrt{E_s/\sigma_{GFDM,v}^2}\right) = Q\left(\sqrt{\gamma/\xi_F}\right), \quad (14)$$

where $\gamma = E_s/\sigma_v^2$ denotes the signal-to-noise ratio (SNR). As shown in (14), the post-equalization SNR of each subsymbol at the receiver is same in GFDM systems. Therefore, achievable rate (AR) of GFDM systems is derived as

$$R_{GFDM} = \log_2(1 + \gamma/\xi_F). \quad (15)$$

III. GFDM ASSISTED NOMA SCHEMES

In [2], multi-carrier NOMA can be considered as a special case of hybrid NOMA, which achieves a tradeoff between system performance and complexity. Sparse code multiple access (SCMA) and pattern division multiple access (PDMA) are two typical examples of multi-carrier NOMA. Specifically, multiple users are divided into several groups in a NOMA network, and user grouping is essential to reach highest performance gain when channel conditions of users in a group are most different. Considering wide applications of OFDM systems, efficient combination of OFDM and NOMA draws lots of attention, such as precoding methods in [13] and power allocation strategies in [14], [15]. However, some shortcomings restrict OFDM systems to be directly employed in 5G networks, especially for low latency and loose synchronization scenarios. As a result, we investigate GFDM assisted NOMA schemes to expand multi-carrier NOMA framework and evaluate combined advantages in comparison with single schemes.

As given in [22], GFDM systems are considered as tradeoff waveforms between OFDM and single carrier systems. Taking LTE for example, single carrier and OFDM systems are employed as uplink and downlink waveforms, respectively. If NOMA networks are introduced to access more users, OFDM based NOMA schemes in [6]–[9] may not be applicable to uplink channels due to large PAPR. Fortunately, GFDM assisted NOMA systems with flexible parameters achieve lower PAPR as well as OOBP performances than OFDM based NOMA systems, and higher transmission rate than GFDM waveforms.

A. BER ANALYSIS FOR DOWNLINK NOMA

In downlink GFDM assisted NOMA schemes, the scenario with one BS and two users is assumed. Different from traditional GFDM systems, each time-frequency resource block is shared by two users, i.e. a near user with less allocated power and a far user with more transmitted power. As shown in Fig.2, considering the SC at the BS, the transmitted signal is expressed as

$$\mathbf{x}_{DL} = \sqrt{\alpha P} \cdot \mathbf{A} \cdot \mathbf{d}_1 + \sqrt{(1-\alpha)P} \cdot \mathbf{A} \cdot \mathbf{d}_2, \quad (16)$$

where $\mathbf{d}_1$ and $\mathbf{d}_2$ denote transmitted signal of U_1 and U_2, respectively. At the user side, the received signal of U_θ is

$$\begin{aligned} \mathbf{y}_\theta &= \mathbf{B} \cdot \mathbf{\Lambda}_\theta^{-1} \cdot (\mathbf{\Lambda}_\theta \cdot \mathbf{x}_{DL} + \mathbf{v}_\theta) \\ &= \sqrt{\alpha P} \cdot \mathbf{d}_1 + \sqrt{(1-\alpha)P} \cdot \mathbf{d}_2 + \mathbf{B} \cdot \mathbf{\Lambda}_\theta^{-1} \cdot \mathbf{v}_\theta, \end{aligned} \quad (17)$$

where $\mathbf{\Lambda}_\theta = \text{diag}([\lambda_{\theta,0}, \lambda_{\theta,1}, \ldots, \lambda_{\theta,N-1}]^T)$ and $\mathbf{v}_\theta$ denote frequency domain responses of fading channels and AWGN with variance σ_v^2 from BS to U_θ, respectively. Without loss of generality, we assume that there is $|\lambda_{1,i}|^2 > |\lambda_{2,i}|^2$. According to (14), the NEF at the receiver should be calculated to derive analytical BER expressions of GFDM assisted NOMA systems. As a result, the NEF at the U_θ side is

$$\xi_\theta = \frac{1}{N} \sum_{k=0}^{N-1} \sum_{i=0}^{N-1} |\mathbf{B} \cdot \mathbf{\Lambda}_\theta^{-1}|_{k,i}^2 = \frac{1}{N} \sum_{k=0}^{N-1} \sum_{i=0}^{N-1} \frac{|\mathbf{B}|_{k,i}^2}{|\lambda_{\theta,i}|^2}. \quad (18)$$

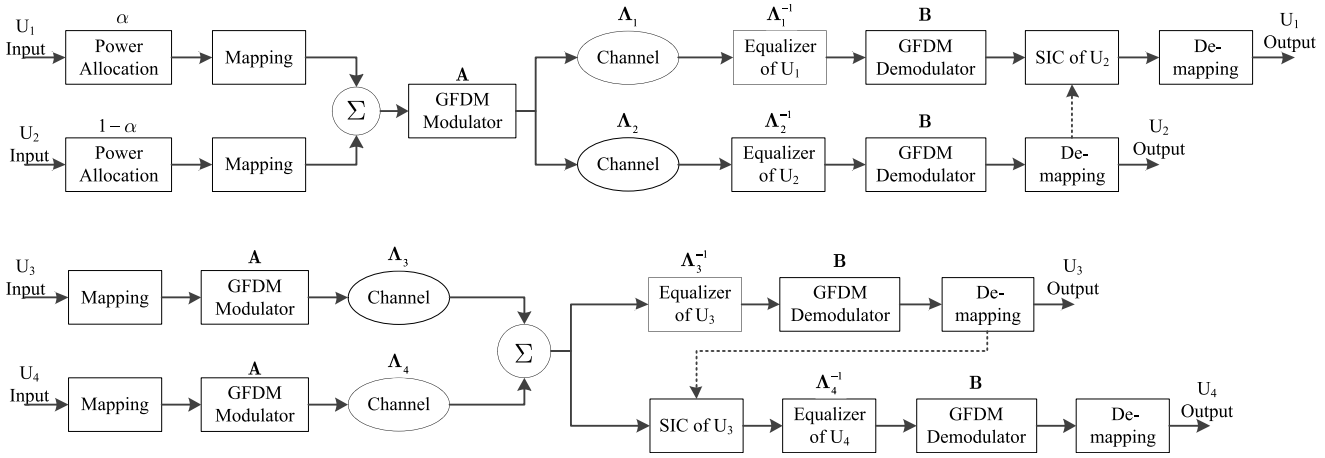

FIGURE 2. The block diagram of downlink and uplink GFDM assisted NOMA schemes.

In NOMA networks, due to greater share of total power, U_2 is first decoded by regarding the signal of U_1 as interference. In most cases, the received signal of U_1 at the U_2 side is completely considered as interference. However, when two users suffer same fading channels and decoding methods, the signal power of U_2 is strengthened or weakened by that of U_1 with 50% probability from the view of theoretical analysis. Therefore, the theoretical BER expression of U_2 is derived as

$$\mathcal{P}_{U_2} = \frac{1}{2}Q\left(\sqrt{\frac{T_1 \cdot \gamma}{\xi_2}}\right) + \frac{1}{2}Q\left(\sqrt{\frac{T_2 \cdot \gamma}{\xi_2}}\right), \tag{19}$$

where ξ_2 is obtained in (18) with $\theta = 2$. Additionally, the power enhancement factor T_1 and power attenuation factor T_2 are denoted as

$$\begin{cases} T_1 = \left(\sqrt{1-\alpha} + \sqrt{\alpha}\right)^2, \\ T_2 = \left(\sqrt{1-\alpha} - \sqrt{\alpha}\right)^2. \end{cases} \tag{20}$$

where $0 < \alpha < 0.5$.

Subsequently, the signal of U_1 can be decoded through employing SIC to remove U_2 from the received signal at the U_1 side, which is expressed as

$$\mathbf{y}_1 = \sqrt{\alpha P} \cdot \mathbf{d}_1 + \sqrt{(1-\alpha)P} \cdot \left(\mathbf{d}_2 - \bar{\mathbf{d}}_2\right) + \mathbf{B} \cdot \mathbf{\Lambda}_1^{-1} \cdot \mathbf{v}_1, \tag{21}$$

where $\bar{\mathbf{d}}_2$ denotes the de-mapping signal of U_2.

As shown in [8], BER performances of U_1 are related with the correct decoding probability of U_2. Actually, the solving of $\mathcal{P}_{U_1}$ can be divided into two aspects. On one hand, if we consider a perfect decoding for U_2 with $\mathbf{d}_2 = \bar{\mathbf{d}}_2$, the BER of U_1 with perfect SIC (PSIC) is equal to that in the case of orthogonal multiple access (OMA), i.e.

$$\mathcal{P}_{U_1-PSIC} = \mathcal{P}_{U_1-OMA} = Q\left(\sqrt{\frac{\alpha \cdot \gamma}{\xi_1}}\right), \tag{22}$$

where ξ_1 is obtained in (18) with $\theta = 1$ and the same power control strategy in (16) is considered. However, it is impossible to achieve perfect decoding of U_2, and thus the results in (22) could be regarded as a BER lower bound of U_1 after using improved SIC methods. On the other hand, the BER of U_1 is obviously deteriorated as a result of wrong demodulation of U_2, i.e. $\mathbf{d}_2 \neq \bar{\mathbf{d}}_2$, which is related to $\mathcal{P}_{U_2}$ in (19).

From the view of superimposed constellation points in [10], the error probability can be calculated through comparing the distance between constellation points and equivalent GFDM noise power, where the distance is decided by the allocated power of two users, i.e. the α. Therefore, analytical BER expression of U_1 in downlink GFDM assisted NOMA schemes is theoretically derived in (23) as shown at the bottom of this page.

B. BER ANALYSIS FOR UPLINK NOMA

As given in Fig.2, the received signal at the BS side for uplink GFDM assisted NOMA schemes is

$$\mathbf{y}_{UL} = \mathbf{\Lambda}_3 \cdot \mathbf{A} \cdot \mathbf{d}_3 + \mathbf{\Lambda}_4 \cdot \mathbf{A} \cdot \mathbf{d}_4 + \mathbf{v}, \tag{24}$$

where $\mathbf{d}_3$ and $\mathbf{d}_4$ denote transmitted signals of U_3 and U_4, respectively. Additionally, $\mathbf{\Lambda}_3$ and $\mathbf{\Lambda}_4$ represent frequency

$$\begin{aligned} \mathcal{P}_{U_1} = {} & Q\left(\sqrt{\frac{\alpha \cdot \gamma}{\xi_1}}\right) + \frac{1}{2}Q\left(2\sqrt{\frac{(1-\alpha)\cdot\gamma}{\xi_2}} + \sqrt{\frac{\alpha\cdot\gamma}{\xi_2}}\right) + \frac{1}{2}Q\left(\sqrt{\frac{(1-\alpha)\cdot\gamma}{\xi_2}} - \sqrt{\frac{\alpha\cdot\gamma}{\xi_2}}\right) \\ & - \frac{1}{2}Q\left(\sqrt{\frac{(1-\alpha)\cdot\gamma}{\xi_2}} + \sqrt{\frac{\alpha\cdot\gamma}{\xi_2}}\right) - \frac{1}{2}Q\left(2\sqrt{\frac{(1-\alpha)\cdot\gamma}{\xi_2}} - \sqrt{\frac{\alpha\cdot\gamma}{\xi_2}}\right). \end{aligned} \tag{23}$$

domain responses of uplink fading channels. As a result of larger power of near user in received signal, U_3 is firstly decoded for uplink GFDM assisted NOMA networks, shown as

$$\begin{aligned}\mathbf{y}_{Fading,U_3} &= \mathbf{d}_3 + \mathbf{B}\cdot\mathbf{\Lambda}_3^{-1}\cdot\mathbf{\Lambda}_4\cdot\mathbf{A}\cdot\mathbf{d}_4 + \mathbf{B}\cdot\mathbf{\Lambda}_3^{-1}\cdot\mathbf{v}\\ &= \mathbf{d}_3 + \mathbf{\Gamma}\cdot\mathbf{d}_4 + \mathbf{B}\cdot\mathbf{\Lambda}_3^{-1}\cdot\mathbf{v},\end{aligned} \tag{25}$$

where $\mathbf{\Gamma} = \mathbf{B}\cdot\mathbf{\Lambda}_3^{-1}\cdot\mathbf{\Lambda}_4\cdot\mathbf{A}$ is jointly decided by channel information of U_3 and U_4. According to [10], theoretical BER for uplink NOMA networks is mathematically analysed for QPSK modulation over AWGN channels, and thus we only derive analytical BER expressions of uplink GFDM assisted NOMA systems over AWGN channels, but obtained results lay the foundation for subsequent research over fading channels. Thus the (25) is simplified as

$$\mathbf{y}_{AWGN,U_3} = \mathbf{d}_3 + \mathbf{d}_4 + \mathbf{B}\cdot\mathbf{v}. \tag{26}$$

In this case, the interference form of $\mathbf{d}_3$ introduced by $\mathbf{d}_4$ is same as that in (17), except the PAF α. Therefore, the signal power of U_3 is strengthened or weakened by that of U_4 with 50% probability, and theoretical BER of U_3 in uplink GFDM assisted NOMA schemes, similar as that in (19), is derived as

$$\mathcal{P}_{U_3} = \frac{1}{2}Q\left(\sqrt{\frac{\gamma_3}{\xi}} + \sqrt{\frac{\gamma_4}{\xi}}\right) + \frac{1}{2}Q\left(\sqrt{\frac{\gamma_3}{\xi}} - \sqrt{\frac{\gamma_4}{\xi}}\right), \tag{27}$$

where $\gamma_3 = P_3/\sigma_v^2$ and $\gamma_4 = P_4/\sigma_v^2$ denote SNR of U_3 and U_4 at the transmitter. In addition, the NEF for AWGN channels can be calculated by (13).

Similar as the case of downlink NOMA networks, the received signal of U_4 after SIC is

$$\mathbf{y}_{AWGN,U_4} = \mathbf{d}_4 + (\mathbf{d}_3 - \bar{\mathbf{d}}_3) + \mathbf{B}\cdot\mathbf{v}, \tag{28}$$

where the BER of U_4 is also influenced by correct decoding probability of U_3.

Following theoretical analysis in [10], the distance between received constellation points is decided by γ_3 and γ_4, not by the PAF α in (23). Consequently, the theoretical BER of U_4 in uplink GFDM assisted NOMA schemes is derived in (29) as shown at the bottom of this page. In addition, if PSIC is assumed to decode data of U_4, i.e. the case of OMA, there is $\mathcal{P}_{U_4-PSIC} = \sqrt{\gamma_4/\xi}$.

C. ACHIEVABLE SUM RATE ANALYSIS

In downlink GFDM assisted NOMA schemes, the achievable rate of U_2, as given in (4), is calculated as

$$R_{GFDM-NOMA,U_2} = \log_2\left(1 + \frac{(1-\alpha)\cdot\gamma}{\alpha\cdot\gamma + \xi_2}\right). \tag{30}$$

As shown in (5), similarly, the achievable rate of U_1 is

$$R_{GFDM-NOMA,U_1} = \log_2\left(1 + \frac{\alpha\cdot\gamma}{\xi_1}\right). \tag{31}$$

Therefore, the achievable sum rate of downlink NOMA networks is obtained as

$$\begin{aligned}&R_{GFDM-NOMA,DL}\\ &= R_{GFDM-NOMA,U_1} + R_{GFDM-NOMA,U_2}\\ &= \log_2\left(1 + \frac{\alpha\cdot\gamma}{\xi_1}\right) + \log_2\left(1 + \frac{(1-\alpha)\cdot\gamma}{\alpha\cdot\gamma + \xi_2}\right).\end{aligned} \tag{32}$$

Correspondingly, for GFDM systems without NOMA, when U_1 and U_2 are successively transmitted on different time-frequency resource blocks, the achievable sum rate with two users is expressed as

$$\begin{aligned}R_{GFDM,DL} &= R_{GFDM,U_1} + R_{GFDM,U_2}\\ &= \beta\log_2\left(1 + \frac{\gamma}{\xi_1}\right) + (1-\beta)\log_2\left(1 + \frac{\gamma}{\xi_2}\right),\end{aligned} \tag{33}$$

where β is the resource allocation coefficient of frequency or time, similar to the PAF α.

IV. SIMULATION RESULTS

In this section, diverse performances, including downlink BER, uplink BER, achievable sum rate, PAPR and OOBP, have been given to illustrate overall characteristics of GFDM assisted NOMA schemes. On one hand, theoretical and simulated BER performances are given for downlink and uplink GFDM assisted NOMA scenarios. On the other hand, compared to OFDM based NOMA systems, advantages of GFDM assisted NOMA schemes are fully shown to achieve better PAPR and OOBP performances. Furthermore, the achievable sum rate of GFDM systems is improved through combining with NOMA schemes.

A. BER PERFORMANCES

BER performances of downlink and uplink GFDM assisted NOMA schemes are illustrated to prove the correctness of theoretical analyses in (19), (23), (27) and (29). In one data block of GFDM systems, there are 128 subcarriers with 5 sub-symbols on one subcarrier. The roll-off parameter of raised cosine filter is $\rho = 0.5$, and QPSK modulation is considered for simulations. The ZF receiver is employed at the receiver.

For the case of downlink GFDM assisted NOMA networks, the relative delay of ITU Veh channels is [0 310 710 1090 1730 2510]ns, and the average power of each path is [0 −1.0 −9.0 −10.0 −15.0 −20.0]dB with maximum Doppler shift 4 Hz. In addition, we presume that the path loss of far user is 3 dB larger than that of near user. Although Rayleigh

$$\mathcal{P}_{U_4} = Q\left(\sqrt{\frac{\gamma_4}{\xi}}\right) + \frac{1}{2}Q\left(2\sqrt{\frac{\gamma_3}{\xi}} + \sqrt{\frac{\gamma_4}{\xi}}\right) + \frac{1}{2}Q\left(\sqrt{\frac{\gamma_3}{\xi}} - \sqrt{\frac{\gamma_4}{\xi}}\right) - \frac{1}{2}Q\left(\sqrt{\frac{\gamma_3}{\xi}} + \sqrt{\frac{\gamma_4}{\xi}}\right) - \frac{1}{2}Q\left(2\sqrt{\frac{\gamma_3}{\xi}} - \sqrt{\frac{\gamma_4}{\xi}}\right). \tag{29}$$

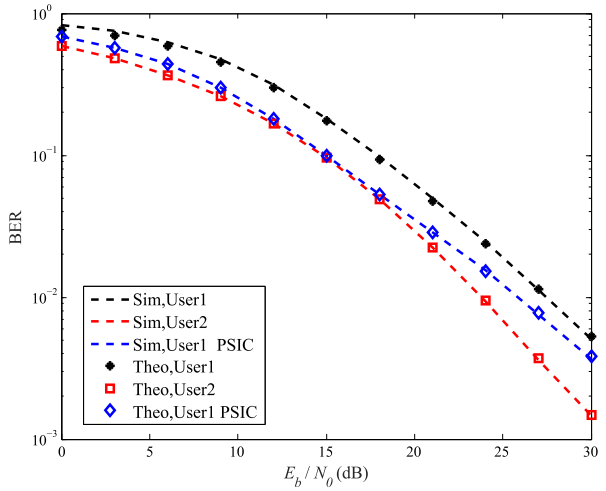

FIGURE 3. BER performances of downlink GFDM assisted NOMA schemes with $\alpha = 0.2$.

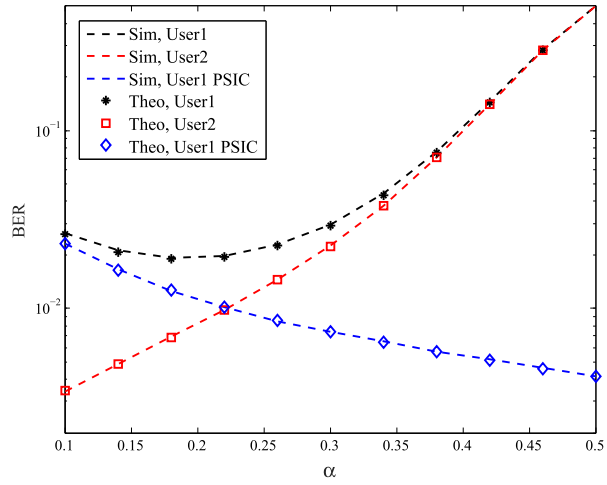

FIGURE 4. BER performances of downlink GFDM assisted NOMA schemes with different α.

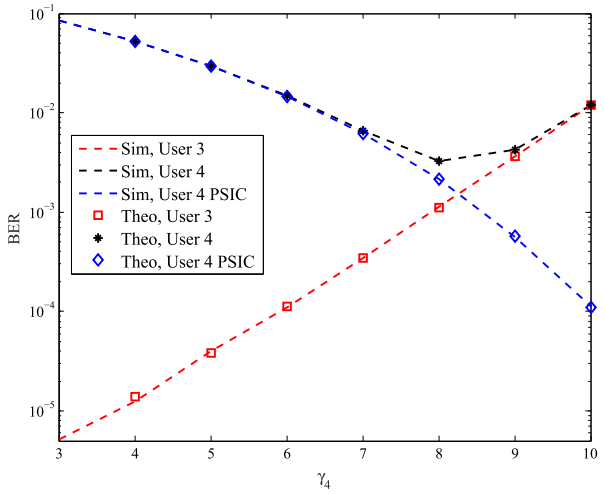

FIGURE 5. BER performances of uplink GFDM assisted NOMA schemes over AWGN channels with different γ_4.

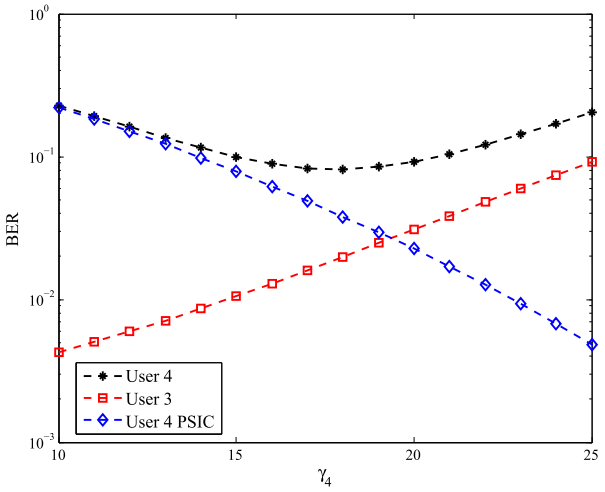

FIGURE 6. BER performances of uplink GFDM assisted NOMA schemes over fading channels with different γ_4.

fading parameters of U_1 and U_2 are same, $\mathbf{\Lambda}_1$ and $\mathbf{\Lambda}_2$ are significantly different to obtain performance gains of NOMA due to the randomness of channels. Simulation results match well with theoretical results, which illustrates the correctness of derived BER expressions in (19) and (23). In Fig. 3, theoretical and simulated BER results with $\alpha = 0.2$ are given. Compared to the case of perfect SIC, BER performances of U_1 are obviously deteriorated due to introduced interference of U_2 for error demodulation. In Fig. 4, theoretical and simulated BER results with $\alpha \in [0.1, 0.5]$ are illustrated. The SNR at the BS is set as $\gamma = 24$ dB. On one hand, BER performances of U_2 are monotonically decreasing with the increase of α and degenerated due to contained interference of U_1. On the other hand, BER performances of U_1 are convex in this interval, where the optimal α could be selected according to a group of given simulation parameters.

For the case of uplink GFDM assisted NOMA networks, BER performances over AWGN and fading channels are given in Fig.5 and Fig.6, respectively. We assume that the path loss of near user is 6 dB less than that of far user. The SNR of U_3 at the user side is $\gamma_3 = 14$ dB for AWGN channels and $\gamma_3 = 30$ dB for fading channels. In Fig.5, theoretical analyses in (27) and (29) are verified correct by the match between theoretical and simulated BER results. The same trend of BER performances over fading channels is shown in Fig.6, where Rayleigh fading parameters are same as those in Fig. 3. Basically, with the increase of γ_4, BER performances of U_3 monotonically drops as a result of more introduced interference. In addition, the BER trend of U_4 is similar as that of U_1 in downlink NOMA, which is also convex in this interval.

B. AR PERFORMANCES

According to (32), achievable sum rate of downlink GFDM assisted NOMA networks is given, which is compared to that of GFDM waveforms with different resource allocation strategies in (33). In Fig.7, AR performances of GFDM waveforms and GFDM assisted NOMA schemes with $\alpha = \beta =$

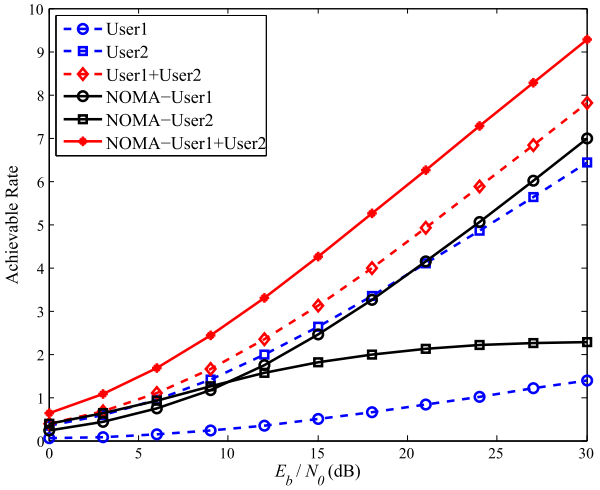

FIGURE 7. Comparison of AR performances between downlink GFDM assisted NOMA networks and GFDM waveforms.

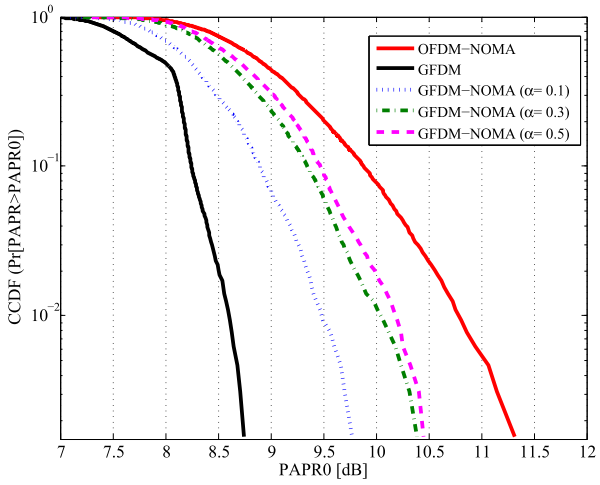

FIGURE 8. Comparison of PAPR performances between downlink GFDM and OFDM based NOMA networks.

0.2 are illustrated. The achievable sum rate of U_1 and U_2 in GFDM assisted NOMA networks is higher than that in GFDM systems, which reflects the advantages of NOMA. For uplink scenarios, achievable sum rate can also be obviously improved through jointing with NOMA networks, which is intuitively illustrated in Fig.2.

C. PAPR AND OOBP PERFORMANCES

Furthermore, we also give PAPR and OOBP results to explain performance advantages of multi-carrier NOMA networks through combining with GFDM waveforms. In Fig.8, we evaluate PAPR performances of GFDM and OFDM based NOMA schemes at the same level of transmitted subsymbols. The GFDM parameters are same as those in Fig.3, and thus there are 640 active subcarriers in OFDM systems. Actually, PAPR of downlink OFDM based NOMA systems is unchanged for different PAF at the BS. Although PAPR of GFDM assisted NOMA schemes becomes higher with the increase of PAF, it is remarkably lower than of OFDM based NOMA systems.

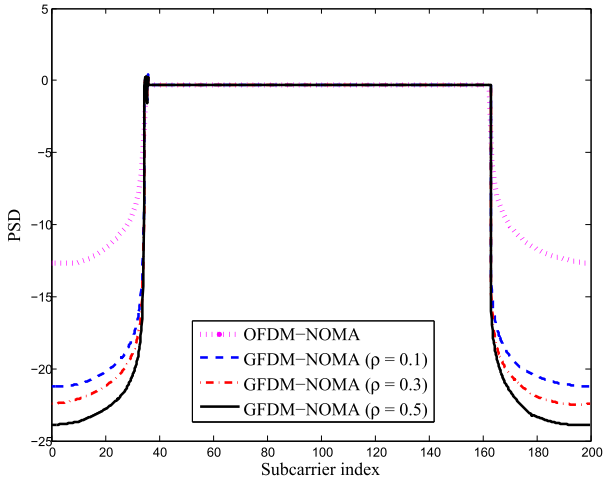

FIGURE 9. Comparison of OOBP performances between GFDM and OFDM based NOMA networks.

In Fig.9, OOBP performances of downlink GFDM and OFDM assisted NOMA networks with $\alpha = 0.2$ are evaluated with the same number of subcarriers, i.e. 128 active subcarriers. Compared to OFDM based NOMA systems, lower OOBP performances are still achieved in GFDM assisted NOMA schemes with diverse roll-off parameters $\rho = 0.1, 0.3, 0.5$. Therefore, combined performance advantages are achieved in GFDM assisted NOMA networks, including higher AR than GFDM waveforms, lower PAPR and OOBP than OFDM based NOMA systems.

V. CONCLUSION

In this paper, we focus on combinations of multiplexing and multiple access techniques in 5G wireless systems. To further extend the research of multi-carrier NOMA, we investigate GFDM assisted NOMA schemes, and then evaluate its theoretical BER performances as well as other essential performances. Specifically, theoretical BER expressions of two users in downlink and uplink GFDM assisted NOMA schemes are derived and verified by simulation results. Additionally, combined advantages of GFDM assisted NOMA schemes are achieved, including higher achievable sum rate than GFDM waveforms, and lower PAPR as well as OOBP performances than OFDM based NOMA systems.

REFERENCES

[1] Y. Liu, Z. Qin, M. Elkashlan, Z. Ding, A. Nallanathan, and L. Hanzo, "Nonorthogonal multiple access for 5G and beyond," *Proc. IEEE*, vol. 105, no. 12, pp. 2347–2381, Dec. 2017.

[2] Z. Ding, X. Lei, G. K. Karagiannidis, R. Schober, J. Yuan, and V. K. Bhargava, "A survey on non-orthogonal multiple access for 5G networks: Research challenges and future trends," *IEEE J. Sel. Areas Commun.*, vol. 35, no. 10, pp. 2181–2195, Oct. 2017.

[3] Y. Cai, Z. Qin, F. Cui, G. Y. Li, and J. A. McCann, "Modulation and multiple access for 5G networks," *IEEE Commun. Surveys Tuts.*, vol. 20, no. 1, pp. 629–646, 1st Quart., 2018.

[4] S. M. R. Islam, N. Avazov, O. A. Dobre, and K.-S. Kwak, "Power-domain non-orthogonal multiple access (NOMA) in 5G systems: Potentials and challenges," *IEEE Commun. Surveys Tuts.*, vol. 19, no. 2, pp. 721–742, 2nd Quart., 2017.

[5] H. Sari, A. Maatouk, E. Caliskan, M. Assaad, M. Koca, and G. Gui, "On the foundation of NOMA and its application to 5G cellular networks," in *Proc. IEEE Wireless Commun. Netw. Conf. (WCNC)*, Apr. 2018, pp. 1–6.

[6] S. Baig, U. Ali, H. M. Asif, A. Ali Khan, and S. Mumtaz, "Closed-form BER expression for Fourier and wavelet transform-based pulse-shaped data in downlink NOMA," *IEEE Commun. Lett.*, vol. 23, no. 4, pp. 592–595, Apr. 2019.

[7] E. C. Cejudo, H. Zhu, and O. Alluhaibi, "On the power allocation and constellation selection in downlink NOMA," in *Proc. IEEE 86th Veh. Technol. Conf. (VTC-Fall)*, Toronto, ON, Canada, Sep. 2017, pp. 1–5.

[8] X. Liu, Y. Wang, F. Zhou, and R. Q. Hu, "BER analysis for NOMA-enabled visible light communication systems with M-PSK," in *Proc. 10th Int. Conf. Wireless Commun. Signal Process. (WCSP)*, Hangzhou, China, Oct. 2018, pp. 1–7.

[9] F. Kara and H. Kaya, "BER performances of downlink and uplink NOMA in the presence of SIC errors over fading channels," *IET Commun.*, vol. 12, no. 15, pp. 1834–1844, Sep. 2018.

[10] X. Wang, F. Labeau, and L. Mei, "Closed-form BER expressions of QPSK constellation for uplink non-orthogonal multiple access," *IEEE Commun. Lett.*, vol. 21, no. 10, pp. 2242–2245, Oct. 2017.

[11] J. S. Yeom, H. S. Jang, K. S. Ko, and B. C. Jung, "BER performance of uplink NOMA with joint maximum-likelihood detector," *IEEE Trans. Veh. Technol.*, vol. 68, no. 10, pp. 10295–10300, Oct. 2019.

[12] J. Zeng, T. Lv, R. P. Liu, X. Su, M. Peng, C. Wang, and J. Mei, "Investigation on evolving single-carrier NOMA into multi-carrier NOMA in 5G," *IEEE Access*, vol. 6, pp. 48268–48288, 2018.

[13] I. Baig, "A precoding-based multicarrier non-orthogonal multiple access scheme for 5G cellular networks," *IEEE Access*, vol. 5, pp. 19233–19238, 2017.

[14] X. Li, C. Li, and Y. Jin, "Dynamic resource allocation for transmit power minimization in OFDM-based NOMA systems," *IEEE Commun. Lett.*, vol. 20, no. 12, pp. 2558–2561, Dec. 2016.

[15] W. Xu, X. Li, C. Lee, M. Pan, and Z. Feng, "Joint sensing duration adaptation, user matching, and power allocation for cognitive OFDM-NOMA systems," *IEEE Trans. Wireless Commun.*, vol. 17, no. 2, pp. 1269–1282, Feb. 2018.

[16] Y. Tao, L. Liu, S. Liu, and Z. Zhang, "A survey: Several technologies of non-orthogonal transmission for 5G," *China Commun.*, vol. 12, no. 10, pp. 1–15, Oct. 2015.

[17] A. Hammoodi, L. Audah, and M. A. Taher, "Green coexistence for 5G waveform candidates: A review," *IEEE Access*, vol. 7, pp. 10103–10126, 2019.

[18] P. Guan, D. Wu, T. Tian, J. Zhou, X. Zhang, L. Gu, A. Benjebbour, M. Iwabuchi, and Y. Kishiyama, "5G field trials: OFDM-based waveforms and mixed numerologies," *IEEE J. Sel. Areas Commun.*, vol. 35, no. 6, pp. 1234–1243, Jun. 2017.

[19] G. P. Aquino and L. Leonel Mendes, "Sparse code multiple access applied in the generalized frequency division multiplexing," in *Proc. IEEE 5G World Forum (5GWF)*, Jul. 2018, pp. 49–54.

[20] M. Mhedhbi and F. E. Boukour, "Analysis and evaluation of pattern division multiple access scheme jointed with 5G waveforms," *IEEE Access*, vol. 7, pp. 21826–21833, 2019.

[21] A. Singh, K. K. Naik, and C. R. S. Kumar, "Impact of SC-FDMA and pilots on PAPR and performance of power domain NOMA-UFMC system," in *Proc. 10th Int. Conf. Ubiquitous Future Netw. (ICUFN)*, Jul. 2018, pp. 507–511.

[22] N. Michailow, M. Matthe, I. S. Gaspar, A. N. Caldevilla, L. L. Mendes, A. Festag, and G. Fettweis, "Generalized frequency division multiplexing for 5th generation cellular networks," *IEEE Trans. Commun.*, vol. 62, no. 9, pp. 3045–3061, Sep. 2014.

[23] Z. Wang, L. Mei, X. Sha, and V. C. M. Leung, "Minimum BER power allocation for space-time coded generalized frequency division multiplexing systems," *IEEE Wireless Commun. Lett.*, vol. 8, no. 3, pp. 717–720, Jun. 2019.

XIAOTONG ZHANG was born in 1977. She received the B.S. and M.S. degrees from the Harbin University of Science and Technology, China. She is currently pursuing the Ph.D. degree with Harbin Engineering University. She possesses deep research experience especially in information and communication systems. She has published two pieces of EI academic articles. She holds one invention patent. Her research interests include spread spectrum communication, signal processing in non-cooperative wireless communication detection, modulation pattern recognition, and 5G waveforms.

ZHENDUO WANG (Member, IEEE) received the B.S., M.S., and Ph.D. degrees in information and communication engineering from the Harbin Institute of Technology, in 2012, 2014, and 2019, respectively. From September 2017 to September 2018, he was a Visiting Scholar with the Department of Electrical and Computer Engineering, The University of British Columbia, Vancouver, BC, Canada. He is currently an Associate Professor with the College of Information and Communication Engineering, Harbin Engineering University, Harbin, China. He has authored or coauthored more than 20 research articles and patents. His research interests include 5G waveforms and transform domain communication systems.

XIAOYAN NING received the B.S. degree in mathematics and applied mathematics and the M.S. and Ph.D. degrees in information and communication engineering from the Harbin Institute of Technology, in 2005, 2007, and 2011, respectively. From September 2015 to September 2016, she was a Visiting Scholar with the University of Delaware. She is currently an Associate Professor with the College of Information and Communication Engineering, Harbin Engineering University, Harbin, China. Her research interests include communication signal processing, physical waveform design, and transform domain communication systems.

HONG XIE was born in 1962. She received the B.S., M.S., and Ph.D. degrees in information and communication engineering from Harbin Engineering University, Harbin, China. She is currently a Professor with the College of Information and Communication Engineering, Harbin Engineering University.